IEEE Access
Multidisciplinary | Rapid Review | Open Access Journal

Received September 1, 2019, accepted October 5, 2019, date of publication October 8, 2019, date of current version October 24, 2019.

Digital Object Identifier 10.1109/ACCESS.2019.2946325

Design and Application of a CT-Based High-Reliability Energy Harvesting Circuit for Monitoring Sensors in Power System

JUE HOU, (Student Member, IEEE), SHAORONG WANG, SHUWEI ZHANG, QIAN SHE, YUXIN ZHU, AND CHENGJING LI

State Key Laboratory of Advanced Electromagnetic Engineering and Technology, School of Electrical and Electronic Engineering, Huazhong University of Science and Technology, Wuhan 430074, China

Corresponding author: Shaorong Wang (wsrwy96@vip.sina.com)

This work was supported by the National Key Research and Development Program of China under Grant 2017YFB0902800.

ABSTRACT This paper presents a current transformer (CT)-based high-reliability energy harvesting circuit (EHC) for an electromagnetic energy extractor, which powers monitoring sensors in power system. Differing from the previous studies on EHC, this study employs only analog electronic components, which makes the EHC both simple and low-cost. Effectively, the EHC accomplishes the integration of surge current protection, power balance adjustment, and auto-sensing controllable startup-running-stop management. Respectively, 1) The EHC bypasses the secondary strong current coupled by primary surge current to protect the load sensor and the EHC itself. 2) The EHC only extracts the needed power by regulating the switching duty cycle in real time so that the harvested power can synchronize with the consumed power. 3) Adopting a segmented voltage control strategy, the EHC could sense the starting condition automatically and start up rapidly. After the starting condition is triggered, the EHC keeps working continuously until it receives the command to stop. Based on theoretical analysis and simulation of the above-mentioned functions, the circuit scheme diagram and the implementation of the EHC are finished. The experimental results indicate that the EHC is reliable and meets the design requirements. In terms of applications, the EHC has been used in the ultra-high voltage shunt compensating capacitor bank (UHV-SCCB) state monitoring sensor units, which reveals that the EHC can operate steadily in any working stage of the monitoring sensor.

INDEX TERMS Current surge protection, energy harvesting circuit, monitoring sensors, power balance adjustment, power management, optimization design.

I. INTRODUCTION

With the development of internet of things (IOT) in smart systems, an increasing number of wireless monitoring sensors are equipped in the power system to accomplish sensor embedment, data sampling, signal processing, and operating state monitoring [1], [2]. The technology of a stable and high-reliability power supply should be diffused as it is indispensable for an online monitoring sensor [3]. Currently, in many application scenarios such as monitoring sensors in HV transmission lines, feeder terminal units (FTUs) in distribution automatic system (DAS), and UHV shunt compensating capacitor bank state monitoring sensors, etc., it is necessary that the energy should be harvested from monitored object to supply power to monitoring sensors due to the limitation of field conditions [4], [5]. Up to now, the energy harvesting methods include: adopting small-capacity high-isolation transformers to extract energy from primary voltage of monitored objects [6]–[8], coupling electric field generated by primary HV system to acquire energy [9]–[12], transforming other forms of local energy that are non-electrical (e.g., solar energy) to electrical energy [13]–[15], and coupling the alternating magnetic field generated by primary current [5], [16]–[20], etc. The employment of each method is determined by actual conditions. This paper focuses on the energy harvesting method of coupling the magnetic field, which is faced with several technical challenges as follows.

Heavy primary short-circuit current caused by short-circuit fault in power system can bring about overvoltage at secondary side of energy harvesting CT, it is therefore

The associate editor coordinating the review of this manuscript and approving it for publication was Jie Tang.

This work is licensed under a Creative Commons Attribution 4.0 License. For more information, see http://creativecommons.org/licenses/by/4.0/

necessary to adopt protective measures to prevent the energy harvesting circuit and the monitoring sensor behind it from being damaged. At present, there are mainly two protection methods. One is to assemble silicon controlled switch (SCS), piezoresistor, gas discharge tube (GDT), and transient voltage suppressor (TVS) to make a surge protection device (SPD) [21]–[23]. The other is to utilize saturation characteristic of energy harvesting CT (protective CT) [24]–[27]. Both methods can achieve the aim of absorbing heavy surge current. However, the former is higher in cost and easier to fail under short-period and repetitive surge, whereas the latter might cause secondary high-frequency surge voltage under the influence of primary surge current, which requires the coordination of other protective circuits.

Without regard to power loss, input power and output power of energy harvesting circuit should match in value [28]. If extracted power is too much, surplus power will be transformed into heat whose accumulation might threaten the safety of circuit. In the opposite case, the monitoring sensor will not be able to function normally. Conventional power supplies in power system are mostly voltage-sourced, whose output power changes with the change of output current. And the energy harvesting CT should be regarded as a current source. Therefore, the strategy of adjusting output voltage is essential for the output power to change as required. In this way, the EHC energy harvesting performance can be optimized.

Due to insufficient primary current, CT might not be able to acquire enough power, and this phenomenon is called ''energy harvesting zero zone'' and may cause the ''false startup'' incident of the EHC. During the ''false startup'' period, the EHC works in a balanced state where secondary voltage and output power are lower than normal values and monitoring sensor fails to start rightly. A general solution to this problem is, first of all, to isolate the monitoring sensor during the start-up period, and then charge such energy storage elements as capacitors and pumps. After both primary current and secondary voltage reach their starting thresholds, then power is exported to monitoring sensor [29]–[32]. Nevertheless, this strategy has to sacrifice the start-up time.

Aiming at the crucial design requirements mentioned above, the paper proposes a CT-based high-reliability EHC for monitoring sensors in power system. The novelties of the EHC could be summarized as the follows: The EHC integrates multiple functions, such as surge current protection, power balance adjustment, and auto-sensing controllable startup-running-stop management. And the EHC employs only analog electronic components, which makes it both simple and low-cost. In application, the EHC has been used in the UHV-SCCB state monitoring sensors.

The rest of the paper is organized as follows: Section II presents the solutions for the purpose of meeting the design requirements, where theoretical analysis and simulation verification are discussed. Section III illustrates the schematic diagram and explains working principle of the EHC. Section IV describes the implementation and showcases the experimental results of the EHC. Section V presents the application and operational tests of the EHC. The paper shall be concluded in Section VI.

II. THEORETICAL ANALYSIS AND SIMULATION

A. ENERGY HARVESTING CT PRIMARY SURGE CURRENT PROTECTION

As shown in Fig. 1, the iron core of CT is designed as toroidal core with high quality silicon steel wound in the rolling direction, which makes the iron core gapless and excellent in magnetic property. In this way, the winding leakage would be negligibly small. The parameters of toroidal core and windings are displayed in Table 1. The toroidal core is rolled by the use of Si-steel strip B27G120 developed by Baosteel Company The inner diameter, outer diameter, and height, are 60mm, 90mm, and 40mm, respectively. The secondary winding copper core's diameter is 0.5mm, its wrapped insulation is heat-resisting fluorinated ethylene-propylene (FEP) resin, and the number of turns is 80.

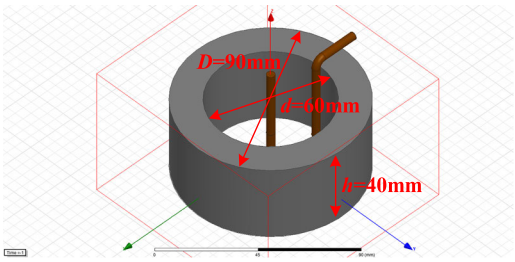

FIGURE 1. Energy harvesting CT 3D model inserted in Ansoft Maxwell.

TABLE 1. Parameters of toroidal core and windings.

The Toroidal Core	External diameter	Inner diameter	Height	Material
	90mm	60mm	40mm	B27G120
The Windings	N_1/N_2	Secondary winding copper core's diameter	Secondary winding's wrapped insulation material	
	1/80	0.5mm	Heat-resisting FEP resin	

The secondary side of energy harvesting CT connects the EHC directly, so the strong current coupled by CT might disturb and damage the back circuit when short-circuit fault occurs in power system. Due to large amplitude of the surge current, the magnetic core of energy harvesting CT can easily enter its saturation zone, which will generate secondary surge voltage threatening the EHC safety. In terms of energy, the surge energy attached to primary surge current will cause the rise of circuit temperature and consequently damage the circuit.

The protection scheme this paper proposes is discussed on the basis of the simplified circuit for surge current protection as shown in Fig. 2. i_1 and i_2 represent primary current and secondary current of energy harvesting CT, respectively. i_1 is superposed by fundamental frequency steady state component $I_{1m}\sin\omega t$ and impulse component i_{pulse}. i_{dc}, i_C and i_R represent rectified DC current, energy storage capacitor current, and load current, respectively. v_{SC} represents

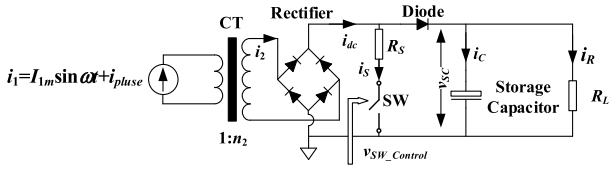

FIGURE 2. Simplified circuit for surge current protection.

storage capacitor voltage. Switch SW and resistor R_S are switch element and small dissipative resistor of bypassing branch, respectively. Capacitor is energy storage and filtering element. The diode prevents power from flowing back to bypassing branch while SW is ON. $v_{SW\_Control}$ is the feedback control signal of SW, whose generation principle will be discussed in Section III. Once v_{SC} monitored in real time reaches protection action value V_{OPT}, SW is turned ON immediately to short-circuit the secondary DC side of energy harvesting CT and then the strong current will be bypassed. Therefore, CT can be treated as working under no-load condition and in its linear region.

Electromagnetic field finite element analysis (FEA) software Ansoft Maxwell developed by ANSYS is equipped with Maxwell Circuit Editor where analog circuit models can be set up and Ansoft Maxwell where 2D/3D models can be inserted to combine magnetic field simulation and circuit simulation. To simulate electromagnetic transient process under the circumstance of primary surge current when the EHC is running normally, energy harvesting CT model as shown in Fig. 1 is constructed in Ansoft Maxwell 3D and a simplified circuit model as shown in Fig. 2 is set up in Maxwell Circuit Editor connected with CT secondary side. Parameters of models are displayed in Table 2.

TABLE 2. Parameters of surge current protection simulation.

Categories	Parameters	Values
Primary Surge Current	I_{1m} and frequency	100A and 50Hz
	I_{pulse} (T_r, P_w, T_f)	2000A (5ms, 10ms 5ms)
Secondary Equivalent Circuit	V_{RET}/V_{OPT}	16V/19V
	R_S	0.125Ω
	Storage Capacitor	6600μF
	R_L	35Ω

In the simulation, the EHC is at first operating normally. The steady-state primary current of energy harvesting CT i_1 equals $I_{1m}\sin\omega t$ and I_{1m} is 100A, frequency is 50Hz. Due to the charging process of capacitor, v_{SC} increases gradually. At $t = 250$ms, the impulse component i_{pulse} whose amplitude I_{pulse}, rise time T_r, pulse width P_w, and fall time T_f are 2000A, 5ms, 10ms, and 5ms, respectively, superposes $I_{1m}\sin\omega t$ as primary current. The simulation waveforms of i_1, i_C, i_{dc}, i_S, and v_{SC} are shown in Fig. 3. It can be observed from the simulation waveforms that at t=250ms, i_C, i_{dc} and v_{SC} increase rapidly because of primary surge current. After about 2ms, v_{SC} increases to $V_{OPT} = 19$V, and SW is turned ON

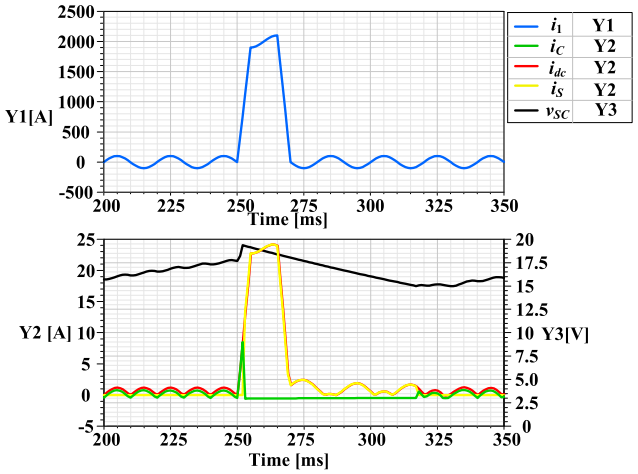

FIGURE 3. The simulation waveforms of i_1, i_C, i_{dc}, i_S, and v_{SC} for surge current protection.

immediately. i_S increases while i_C decreases suddenly. The coupled strong current is bypassed by the branch composed of R_S and SW in series. While SW keeps ON, waveforms of i_{dc} and i_S overlap with each other, which demonstrates that the strong current coupled to secondary side is bypassed completely. Since storage capacitor discharges and supplies power to R_L, v_{SC} decreases gradually. When v_{SC} drops to $V_{RET} = 15$V, SW is turned OFF and the EHC returns to normal operation.

The foregoing analysis and simulation have shown that the proposed surge current protection adopts a bypassing branch, which is designed to be placed at the secondary DC side of energy harvesting CT. By means of feedback control, the EHC is able to short-circuit the above-mentioned branch to prevent overvoltage from damaging the back circuit. And the protection branch, which can withstand short-period repetitive surge, can be realized easily by employing analog elements and multi-branches in parallel.

B. EHC POWER BALANCE ADJUSTING PRINCIPLE AND ENERGY HARVESTING CAPACITY OPTIMIZATION

Currently, the analytical method of harvested energy based on CT is the traditional impedance matching method, whose basic train of thought can be concluded as the following: Based on equivalent vector diagram and circuit model, harvested power P_L's theoretical equation with primary current I_1, secondary voltage V_2, and load R_L, etc., shall be derived. It can be concluded that P_{Lmax} is only related to R_L, which means only when R_L matches the load value of P_{Lmax} can CT extract most of the power. However, in practice, R_L changes along with monitoring sensor's running condition, which requires the change of P_L. Hence, traditional impedance matching method is not suitable for analyzing the power balance problem. The correct train of thought should be as follows: Adjusting the EHC harvested power (input power) in real time to make it follow load consumed power (output power), which helps the EHC to "extract power as needed". In this paper, based on the simplified circuit as

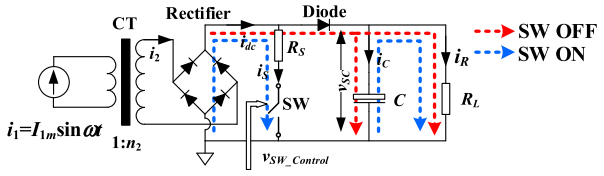

FIGURE 4. Simplified circuit for power balance adjustment.

shown in Fig. 4, the capacitor is used as energy storage element and controls SW so as to adjust input power of the EHC. SW is turned ON when v_{SC} reaches V_{OPT} and is turned OFF when v_{SC} drops to V_{RET}.

In Fig. 4, all physical quantities are the same as those in Fig. 2 except $i_1 = I_{1m}\sin\omega t$ without impulse component, which results in $i_{dc} = |i_1/n_2| = I_{1m}|\sin\omega t|/n_2$. The blue dotted arrows represent the power flow when SW is ON and the red ones represent the power flow when SW is OFF. Assuming I_{1m} and R_L remain constant during a switching period T, which includes switching-on duration t_{on} and switching-off duration t_{off}, charging power of capacitor is decided by i_C, v_{SC}, and t_{off}. Meanwhile, i_C is decided by i_1 and is hard to control directly, so it is rather inconvenient to control v_{SC} and t_{off} for adjusting input power. Therefore, t_{off} is regulated to adjust power balance and v_{SC} is regulated to optimize energy harvesting ability of the EHC. Based on the model shown in Fig. 4, theoretical expressions of t_{on} and t_{off} are derived as follows.

While SW is ON, storage capacitor discharges and $i_{dc} = i_S$, $i_C = -i_R$. Equation (1) shows circuit differential equation and Equation (2) shows initial condition when SW is ON. Equation (3) shows solution of $v_{SC}(t)$ and Equation (4) shows solution of t_{on}.

$$C\frac{dv_{SC}}{dt} = -\frac{v_{SC}}{R_L} \tag{1}$$

$$v_{SC}(0_+) = v_{SC}(0_-) = V_{OPT} \tag{2}$$

$$v_{SC}(t) = V_{OPT}e^{-\frac{t}{R_LC}}(t \geq 0) \tag{3}$$

$$t_{on} = -R_LC\ln\frac{V_{RET}}{V_{OPT}} \tag{4}$$

$$C\frac{dv_{SC}}{dt} + \frac{1}{R_L}v_{SC} = \frac{I_{1m}}{n_2}\sin\omega t \tag{5}$$

$$v_{SC}^{(1)}(0_+) = v_{SC}^{(1)}(0_-) = V_{RET} \tag{6}$$

$$\begin{aligned} v_{SC}^{(1)}(t) = {} & \frac{I_{1m}\omega R_L^2 C}{n_2(1+\omega^2R_L^2C^2)}(\cos\omega t - \frac{1}{\omega R_LC}\sin\omega t) \\ & + \frac{I_{1m}\omega R_L^2 C}{n_2(1+\omega^2R_L^2C^2)}e^{-\frac{t}{R_LC}} \\ & \times (0 \leq t \leq 10\text{ms}) \end{aligned} \tag{7}$$

$$\begin{aligned} t_{off} &= T^{(1)} + T^{(2)} + \ldots + T^{(n)} \\ &= 10(n-1) + T^{(n)}(\text{ms}) \end{aligned} \tag{8}$$

While SW is OFF, $i_{dc} = i_R + i_C$. This period can be split into $T^{(1)}$, $T^{(2)}$, …, and $T^{(n)}$ as shown in Fig. 5 (a). Fig. 5 (b) shows the theoretical waveforms of v_{SC}, i_{dc}, i_C, and i_R in the i^{th} period $T^{(i)}$.

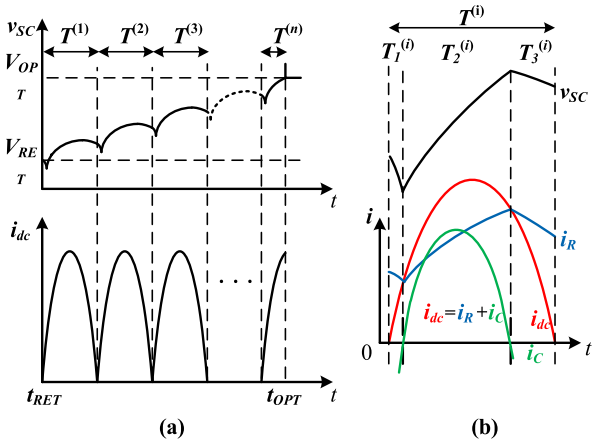

FIGURE 5. Theoretical waveforms of v_{SC}, i_{dc}, i_R, and i_C when SW is OFF: (a) Theoretical waveforms of v_{SC} and i_{dc} in whole SW OFF period, (b) Theoretical waveforms of v_{SC}, i_{dc}, i_R, and i_C in the i^{th} period $T(i)$.

During $T_1^{(i)}$ and $T_3^{(i)}$, i_{dc} is too small to supply load, so the capacitor discharges, resulting in $i_{dc} < i_R$. During $T_2^{(i)}$, i_{dc} is big enough to fulfill load and to charge the capacitor, so $i_{dc} > i_R$. Hence, storage capacitor alternates itself with charging and discharging. Equation (5) shows circuit differential equation and Equation (6) shows initial condition in $T^{(1)}$. Equation (7) shows solution of $v_{SC}{}^{(1)}(t)$ in $T^{(1)}$. Then $t = 10$ms is substituted into (7) and the initial condition of $T^{(2)}$ can be solved, which is then substituted into (5) and solution of $v_{SC}{}^{(2)}(t)$ can be determined, and so on. After the n^{th} iteration, $v_{SC}{}^{(n)}(0+) > V_{OPT}$, the equation $v_{SC}{}^{(n)}(t) = V_{OPT}$ is solved to determine $T^{(n)}$ and the solution of t_{off} is shown in Equation (8).

It is obvious that t_{off} is determined by I_{1m}, R_L, V_{OPT}, and V_{RET}, which makes the input power follow the output power and the EHC accomplish power balance adjustment. Input current effective value I_{1rms} and output power P_L represent the external condition of the EHC. After the theoretical expressions of t_{on} and t_{off} are derived, simulations are conducted to verify theoretical analysis. Fig. 6 shows simulation waveforms under the circumstance of $V_{RET}/V_{OPT} = 15/19$V and $I_{1rms} = 67.7$A $P_L = 8$W ($R_L = 36.125\Omega$), whose t_{on} and t_{off} coincide with the theoretical ones. Table 3 lists

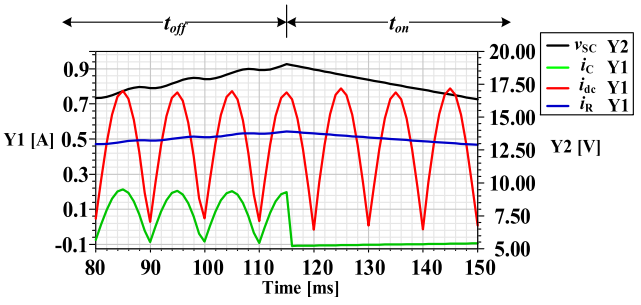

FIGURE 6. Simulation waveforms of v_{SC}, i_{dc}, i_R, and i_C under the circumstance of $V_{RET}/V_{OPT} = 15/19$V and $I_{1rms} = 67.7$A $P_L = 8$W.

TABLE 3. Contrast between theoretical results and simulation results.

Running Conditions	Theoretical Results	Simulation Results
V_{RET}/V_{OPT}=15/19V	t_{on}=57ms	t_{on}=57ms
I_{1rms}=67.7A P_L=8W	t_{off}=126ms	t_{off}=110ms
V_{RET}/V_{OPT}=15/19V	t_{on}=57ms	t_{on}=57ms
I_{1rms}=88A P_L=8W	t_{off}=65ms	t_{off}=54ms
V_{RET}/V_{OPT}=15/19V	t_{on}=151ms	t_{on}=154ms
I_{1rms}=88A P_L=3W	t_{off}=37ms	t_{off}=34ms

theoretical and simulation results of t_{on} and t_{off} in three running conditions and it can be observed from the contrast that they are basically corresponding and I_{1rms} and P_L are negatively correlated with t_{off} and t_{on}, respectively.

Switching duty cycle $D = t_{off}/(t_{on}+t_{off})$ is used as an index to evaluate working condition of the EHC. The closer D is to 0, the longer t_{off} is than t_{on}, which means I_{1m} is bigger, P_L is smaller and the energy can be harvested more easily. On the contrary, harvesting the energy might be harder. Therefore, analyzing variation of D under different V_{RET}/V_{OPT} while I_{1rms} and P_L remain constant has reference value to enhancing the EHC energy harvesting ability. Apparently, modulating V_{RET}/V_{OPT} for D_{min} to attain the optimal energy harvesting capacity is significant.

The plot shown in Fig. 7 shows the trend of switching duty cycle D under different V_{OPT} and V_{RET} under the condition of $I_{1rms} = 88$A and $P_L = 3$W. It is apparent that the larger V_{OPT} and V_{RET} are, the smaller D is. Hence, it can be concluded that the larger the modulation of V_{OPT} and V_{RET} are, the EHC can extract energy more easily, the larger P_{Lmax} is while $I_{1\mathrm{rms}}$ is constant, the smaller minimum primary current that meets energy harvesting requirement is while P_L is constant, and the wider the primary current range is. All in all, the switching duty cycle D provides a quantitative analytical method of the EHC energy harvesting state, based on which V_{RET}/V_{OPT} are modulated as 15/19V to optimize the energy harvesting ability.

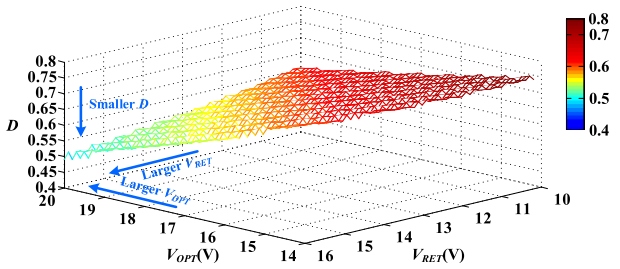

FIGURE 7. Trend of switching duty cycle D under different V_{OPT} and V_{RET}.

A highly efficient self-powered sensor with a radio-frequency (RF) transmission range of a few hundred miters is presented in [33], whose power balance runs in pulsed mode operation which is similar to that in the EHC. The differences lie in the order of magnitudes of the harvested power and the switching mode. According to the calculating methods in [33], the harvested power conversion efficiency of the EHC can be calculated as 45% among the three experiments in Table 3.

C. EHC AUTO-SENSING CONTROLLABLE STARTUP-RUNNING-STOP MANAGEMENT

The essence of "false startup" problem should be concluded as: During start-up period, DC voltage fails to reach the starting threshold. At the same time, the load begins to consume energy. Although load has not started completely, a sub-balanced state has been set up between the EHC and the load. Also, the slowly growing DC voltage is closely related to start-up time as well. The solution to this problem suggested in this paper takes full advantage of the terminal voltage of back-up source. The back-up source plays an important role in interruption-free power supply of monitoring device in power system [34], [35]. Based on the simplified circuit shown in Fig. 8, a segmented voltage control strategy using battery voltage as supporting voltage makes the EHC realize rapid startup, self-hold running, controlled stop, and power management.

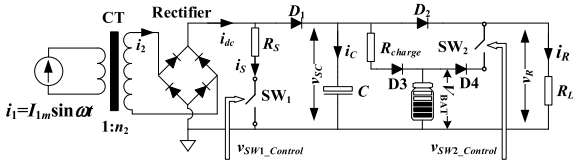

FIGURE 8. Simplified circuit for segmented voltage control strategy.

The simplified circuit shown in Fig. 8 is an extended model of the one shown in Fig. 4. Physical quantities like i_1, i_2, i_{dc}, i_S, i_C, i_R, v_{SC}, and v_R are the same as those in Fig. 4. Differences lie in the additional elements like diode $D_2 \sim D_4$ which are used to restrict power flow's distance and R_{charge} which is placed to realize floating charge of battery. The EHC monitors v_{SC} in real time and controls SW_1 and SW_2 to regulate v_{SC} and v_R. Based on segmented voltage control principle, v_{SC}'s reference values ranging from small to large are battery start-up voltage V_{BAT_STR}, battery terminal voltage V_{BAT}, returned voltage V_{RET}, and operating voltage V_{OPT}. Fig. 9 shows theoretical waveforms of v_{SC}, v_R, $v_{SW1\_Control}$, and $v_{SW2\_Control}$ in the whole process of the EHC start-running-stop. When v_{SC} reaches V_{BAT_STR}, SW_2 is turned ON immediately to discharge battery, which makes v_R increase promptly and load start normally. Obviously, V_{BAT_STR} shall

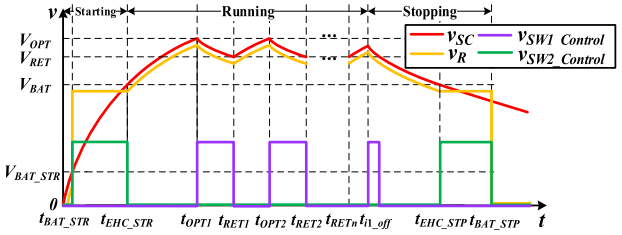

FIGURE 9. Theoretical waveforms of v_{SC}, v_R, $v_{SW1\_Control}$, and $v_{SW2\_Control}$ in the whole process of EHC startup-running-stop.

be as low as possible to shorten t_{BAT_STR}. At t_{EHC_STR}, v_{SC} reaches V_{BAT} and the harvested energy shall charge battery and supply load, SW_2 is turned OFF. After t_{OPT1}, v_{SC} is limited between V_{OPT} and V_{RET}, SW_1 is ON and OFF in alternation. At t_{i1_off}, i_1 is cut off and v_{SC} starts to fall down gradually due to the discharging of capacitor. At t_{EHC_STP}, v_{SC} drops to V_{BAT}, SW_2 is turned ON and battery power replaces the harvesting energy to supply R_L. At t_{BAT_STP}, SW_2 turns OFF and the EHC stops completely.

Fig. 10 shows simulation waveforms of v_{SC}, v_R, $v_{SW1\_Control}$, and $v_{SW2\_Control}$ in the whole process of the EHC start-running-stop. In the simulation, reference voltages and primary current are set as follows: $V_{BAT_STR} = 0.8$V, $V_{BAT} = 12$V, $V_{RET} = 15$V, $V_{OPT} = 19$V, and $I_{1m} = 100$A. Accordingly, $t_{BAT_STR} = 0.006$s, $t_{EHC_STR} = 0.082$s, $t_{i1_off} = 1$s, $t_{EHC_STP} = 1.676$s, and $t_{BAT_STP} = 2.5$s. In this case, start-up time is shortened from 82ms to 6ms by 76ms. Due to tiny primary current and secondary voltage start-up thresholds, start-up time is greatly shortened. Also, "false startup" problem is solved because of the battery support during the start-up period, which makes the EHC segmented voltage control method fit for application scenario that has a high demand on the short start-up time. After the start-up is finished, the harvested energy is distributed to capacitor storage energy, battery energy, and load consuming energy effectively to realize the EHC power management.

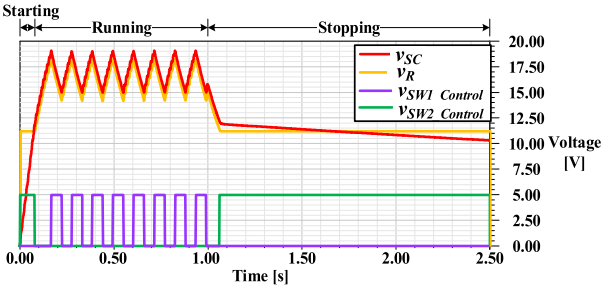

FIGURE 10. Simulation waveforms of v_{SC}, v_R, $v_{SW1\_Control}$, and $v_{SW2\_Control}$ in the whole process of EHC startup-running-stop.

Therefore, in the whole startup-running-stopping period, the usage of battery would be as follows: a) During the EHC startup period, battery would only provide supporting voltage in a period as short as tens of milliseconds. b) Battery would be floating charged in the running period. c) Under the circumstance of fault and action of relay protection, battery would be operated to quit running after the whole transient process is recorded by sensors to prevent itself from being used up. Therefore, the battery would not be consumed very much, and its service life could be extended as long as possible.

III. CONFIGURATION AND CONTROL PRINCIPLE OF EHC

Schematic circuit diagram of the EHC shown in Fig. 11 is composed of energy harvesting CT, rectifier circuit, voltage regulating and protecting circuit, energy storing circuit, voltage regulating and protecting controlling circuit, EHC start-stop and battery controlling circuit, and DC-DC. i_2, i_2 and i_{dc} represent primary current, secondary current and rectified current, respectively. i_{dc_int} is intermittent current with harmonic due to voltage regulating and protecting circuit. i_{dc_cnt} is continuous current under the influence of energy storing circuit. i_{dcdc_in} represents the input current of DC-DC. v_{GS}, v_{SC}, v_{dcdc_in}, V_{OUT} and V_{BAT} are driving voltage of NMOS Q_1 and Q_2, storage capacitor voltage, input voltage of DC-DC, output voltage of DC-DC, and battery voltage. The EHC electrical characteristics are shown in Table 4.

TABLE 4. EHC electrical characteristics.

Parameters	Symbols	Values	Unit
Rated primary current effective value	I_{1rms}	80	A
Maximum surge current	I_{pulse_max}	2500	A
Maximum output power	P_{Lmax}	12	W
Minimum primary current/under different P_L	I_{1min}	65A/10W, 52A/8W, 43A/5W, 10.7A /1W, 8.5A/50mW	A
Battery start-up voltage	V_{BAT_STR}	0.8	V
Battery terminal voltage	V_{BAT}	12	V
Output voltage of DC-DC	V_{OUT}	5	V
Returned regulating voltage	V_{RET_1} V_{RET_2}	15 22	V
Operating voltage	V_{OPT_1} V_{OPT_2}	19 26	V
Start-up time	t_{BAT_STR}	5	ms

The alternating magnetic field converges in toroidal core of energy harvesting CT, which leads the winding to generate secondary voltage. The dissipative resistors $R_1 \sim R_4$ (0.5Ω/2W) connect NMOS Q_1 and Q_2 in series to constitute voltage regulating and protecting circuit, which has the functions of surge current protection, power balance adjustment, and v_{SC} regulation. Q_1 and Q_2 are feedback controlled by voltage regulating and protecting controlling circuit, whose driving voltages are v_{SC} and v_{DCDC_IN}. Generally, Q_1 and Q_2 alternate between ON and OFF to adjust power balance and regulate v_{SC} within the limits of $V_{RET} \sim V_{OPT}$. As short-circuit current occurs at primary side, Q_1 and Q_2 are turned ON immediately to bypass surge current. In energy storing circuit, capacitors C_1 and C_2 (3300μF/64V) are in parallel with discharge resistors R_6 and R_7 (3kΩ/0.25W). Diode D_5 prevents the stored power of capacitors from flowing back. Voltage regulating and protecting controlling circuit, whose working flow diagram is shown in Fig. 12 (a), consists of BJT Q_3 and Q_4, $R_8 \sim R_{14}$, and $D_7 \sim D_{13}$. Topologies and connections of first-stage protecting controlling circuit and second-stage protecting controlling circuit are the same (only first-stage circuit is shown in Fig. 11). But the voltage adjusting modulation values are different as shown in Table 4 and V_{RET} and V_{OPT} can be modulated by adjusting R_9 and R_{10}, respectively. The EHC start-stop and battery controlling

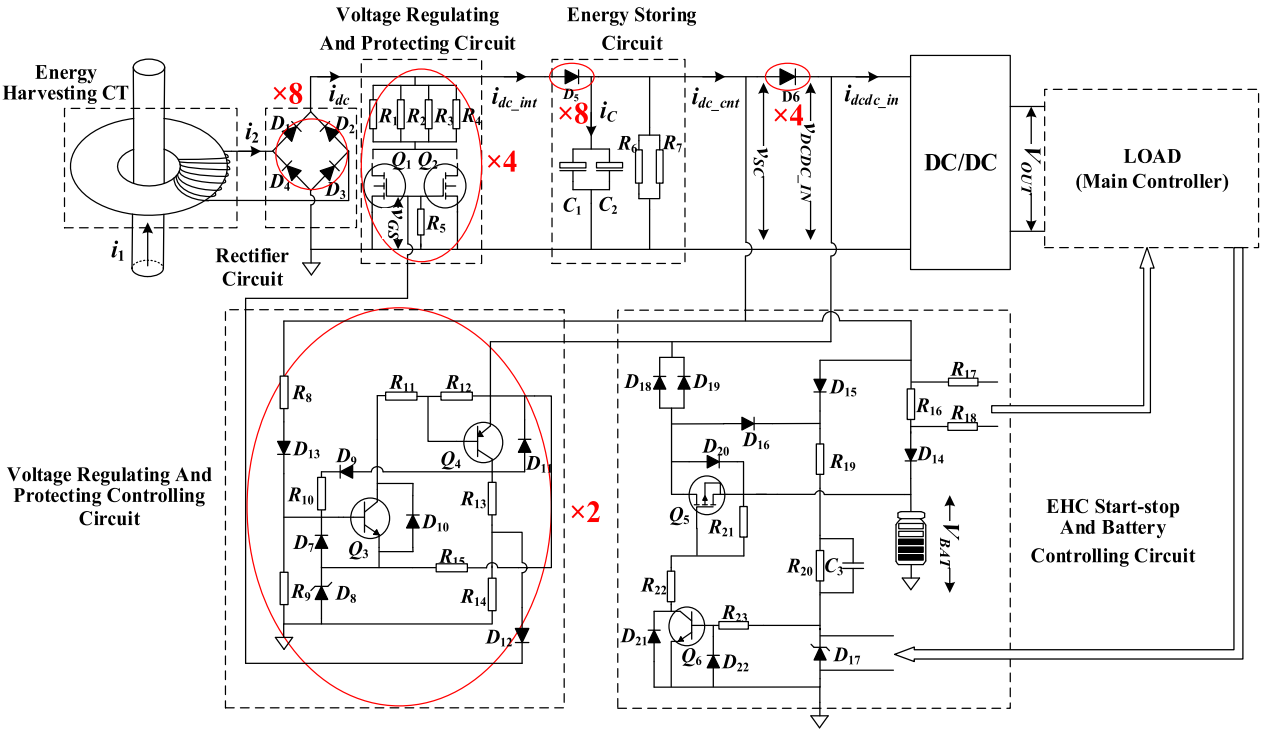

FIGURE 11. Schematic circuit of EHC.

circuit, whose working flow diagram is shown in Fig. 12 (b), is composed of PMOS Q_5, BJT Q_6, speed-up capacitor C_3, $R_{16} \sim R_{23}$, $D_{14} \sim D_{22}$, and battery. And it makes the EHC realize the functions of rapid startup, self-hold running, and controlled stop. Diode D_6 prevents battery power from flowing back.

DC-DC module power provides steady DC voltage to monitoring sensor.

It should be pointed out that for the sake of withstanding secondary transient overcurrent, the EHC adopts multiple elements and branches in parallel such as 8 diodes in each rectifier bridge arm, 4 branches in voltage regulating and protecting circuit, 8 diodes of D_5, 4 diodes of D_6, and two-stage design in voltage regulating and protecting controlling circuit.

The EHC's rated primary current effective value I_{1rms} and the maximum output power P_{Lmax} are set to be 80A and 12W as shown in Table 4. Besides, it should be pointed out that the minimum primary current (I_{1min}) is a relative value, which is related to the load consuming power P_L. And with the decrease of the consumed power, I_{1min} would decrease furthermore. For instance, $P_L = 10$W $I_{1min} = 65$A, $P_L = 8$W $I_{1min} = 52$A, $P_L = 5$W $I_{1min} = 43$A, $P_L = 1$W $I_{1min} = 10.7$A, $P_L = 50$mW $I_{1min} = 8.5$A. As long as I_1 is greater than I_{1min}, sufficient energy would be supplied by EHC. Also, because harvested power would follow the consumed power synchronously, no energy would be wasted.

In the EHC, leakage current exists in the board prototype due to the controlling branches, discharging resistors in parallel with capacitor, and charging branch of battery, etc. Due to the power balance adjustment, the DC voltage of the EHC would fluctuate between 15V to 19V, which makes the leakage current fluctuate within a small range, too. The leakage current could be calculated by subtracting the measured load current from the current in the DC side of rectifier circuit using Multisim 14.0. When battery is in the state of floating charge, the leakage current fluctuates between 50mA and 80mA that accounts for about 10%∼12% of the DC current when the EHC extracts 10W power to load. Besides, with the increase of the primary current, the proportion would further decrease.

IV. IMPLEMENTATION AND EXPERIMENTS RESULT

A. EXPERIMENTAL PLATFORM AND IMPLEMENTATION OF EHC

For the purpose of verifying the feasibility of the EHC design, an experimental platform is established in laboratory as shown in Fig. 13 (a). About energy harvesting CT, the toroidal core is rolled by Si-steel strip B27G120 developed by Baosteel Company The inner diameter, outer diameter, height, and cross sectional area are 60mm, 90mm, 40mm, and 600mm^2, respectively. The secondary winding copper core's diameter is 0.5mm, and its wrapped insulation is heat-resisting FEP resin. The number of turns is 80. The battery made by Panasonic is LC series small back-up source battery LC-P121R3P. The URB_MP-12W series DC-DC converter developed by MORNSUN is used as DC-DC, whose input voltage ranges from 9∼36V and output voltage is 5V.

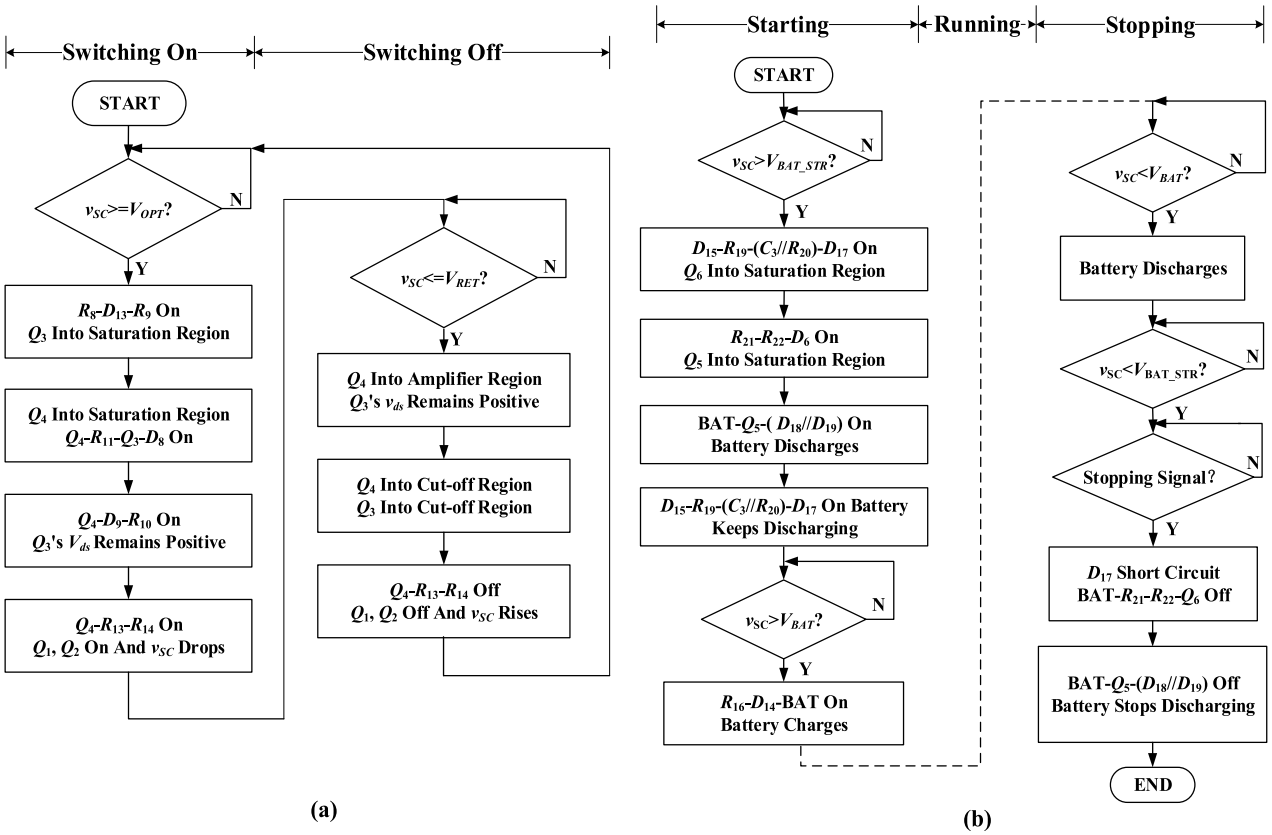

FIGURE 12. Working flowcharts of voltage regulating and protecting controlling circuit and EHC start-stop and battery controlling circuit: (a) Working flowchart of voltage regulating and protecting controlling circuit, (b) Working flowchart of EHC start-stop and battery controlling circuit.

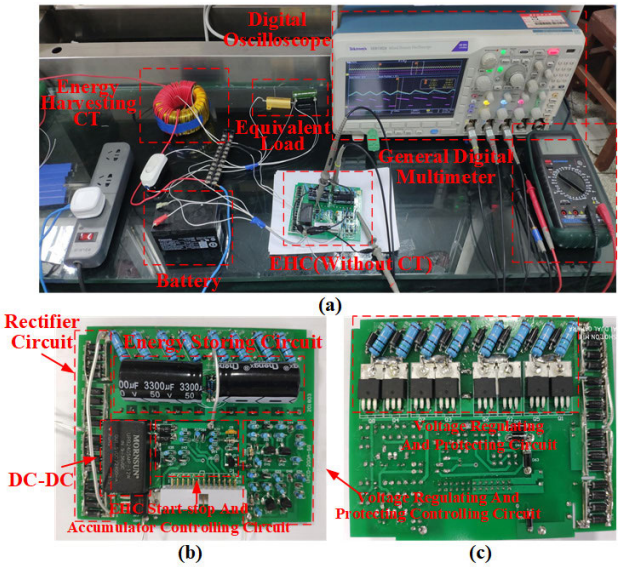

FIGURE 13. Photos of the experimental environment and PCB of EHC: (a) Photo of experimental platform, (b) Photo of top side of PCB, (c) Photo of bottom side of PCB.

The PCB of the EHC, which adopts discrete components and blocking layout, is displayed in two-side view in Fig. 13 (b) and Fig. 13 (c).

B. EHC POWER BALANCE ADJUSTING EXPERIMENTS

To verify the EHC power balance adjusting principle this paper presented, experiments of power balance adjustment are conducted. The running condition of the EHC is changed by altering effective value of primary current I_{1rms} and output power P_L. Then, the waveforms of storage capacitor voltage v_{SC}, DC-DC input voltage mv_{DCDC_IN}, and driving voltage v_{GS} of Q_1 and Q_2 are recorded as shown in Fig. 14 to compare the EHC power balance adjustment in three different running conditions. Because P_L is decided by load voltage U_L and load current I_L and load voltage keeps constant as 5V, I_L changes along with P_L. Therefore, waveforms of I_L are not recorded in Fig. 14. The yellow curve represents v_{SC}, the blue curve refers to v_{DCDC_IN}, and the purple curve is v_{GS}. At the time when the cursor points to *a* as shown in Fig. 14 (a) and (b), I_{1rms} changes from 66.7A to 88A while P_L keeps 8W. At the time when the cursor points to *b* as shown in Fig. 14 (a) and (c), P_L changes from 8W to 3W while I_{1rms} keeps 88A. t_{on} and t_{off} in every condition are measured to verify theoretical and simulation analysis. Table 5 shows the comparison of simulation results with experiment ones in the three conditions mentioned above. It can be seen from Table 5 that t_{on} decreases while I_{1rms} increases, t_{off} increases while P_L decreases. Also, it can be found that t_{on} and t_{off} in theoretical calculation, simulation, and experimental

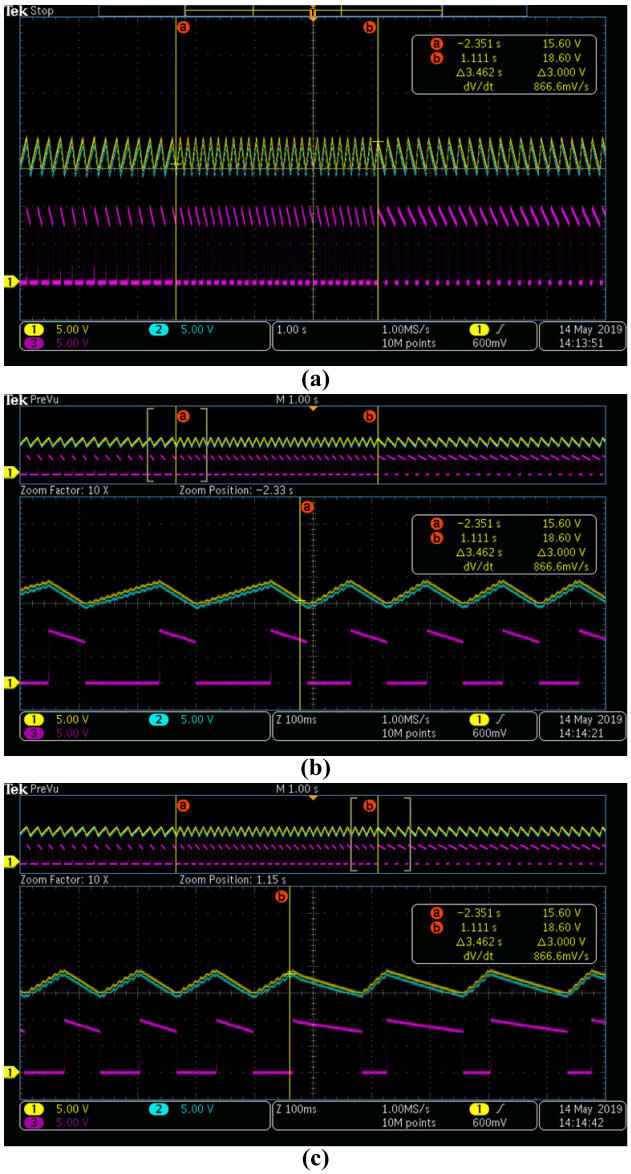

FIGURE 14. Measured waveforms of v_{SC}, v_{DCDC_IN}, v_{GS} under EHC power balance adjustment: (a) Whole waveforms in three conditions, (b) Part of waveforms while running condition is switched from 1 to 2, (c) Part of waveforms while running condition is switched from 2 to 3.

TABLE 5. Comparison between simulation results and experiment results in different running conditions.

No.	Running Conditions	Simulation Results	Experiment Results
1	I_{1rms}=67.7A P_L=8W	t_{off}=110ms t_{on}=57ms D=0.66	t_{off}=125ms t_{on}=64ms D=0.66
2	I_{1rms}=88A P_L=8W	t_{off}=54ms t_{on}=57ms D=0.49	t_{off}=62ms t_{on}=64ms D=0.49
3	I_{1rms}=88A P_L=3W	t_{off}=34ms t_{on}=154ms D=0.18	t_{off}=38ms t_{on}=140ms D=0.21

measurement are basically the same, which means that the power balance adjustment of the EHC is effective and fulfills the change of the output power as required.

C. EHC AUTO-SENSING CONTROLLABLE STARTUP-RUNNING-STOP MANAGEMENT EXPERIMENTS

To verify the EHC auto-sensing controllable startup-running-stop management, the experiments of segmented voltage control principle are conducted, in which $I_{1rms} = 88$A, $P_L = 5$W. The reference values of v_{SC} ranging from small to large are $V_{BAT_STR} = 0.8$V, $V_{BAT} = 12$V, $V_{RET} = 15$V, and $V_{OPT} = 19$V. The EHC experiences start, running, and stop and the waveforms of v_{SC}, v_{DCDC_IN}, and v_{GS} are recorded as shown in Fig. 15. The yellow curve represents v_{SC}, the blue curve represents v_{DCDC_IN}, the purple curve represents driving voltage v_{GS} of Q_1 and Q_2.

In the start-up period as shown in Fig. 15 (b), at the time when the cursor points to a, v_{SC} reaches V_{BAT_STR} and

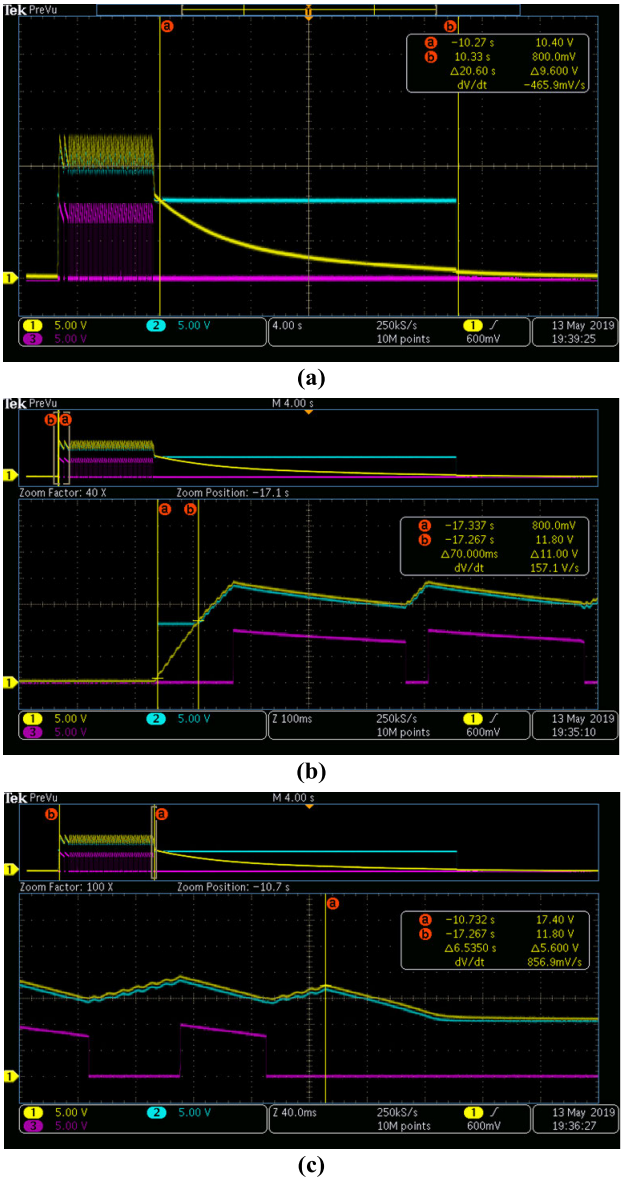

FIGURE 15. Measured waveforms of v_{SC}, v_{DCDC_IN}, v_{GS} in the process of a whole start-running-stop of EHC when $I_{1rms} = 88$A, $P_L = 5$W: (a) Waveforms in the whole process, (b) Part of waveforms during start-up period, (c) Part of waveforms while primary current is cut off.

battery starts to discharge, which leads v_{DCDC_IN} increases to approach V_{BAT}. At the time when the cursor points to b, v_{SC} reaches V_{BAT} and the harvested energy replaces battery power to supply equivalent load. Δt measured between cursor a and cursor b is 70ms, which indicates that the EHC realizes the function of rapid startup, and the start-up time is shortened by 70ms, which basically fills up the first charge time of storage capacitor. The start-up time under this condition is about 5ms. If monitor sensor has the function of fault recording, the headmost three and a half cycles can be recorded. At the time when the cursor points to a as shown in Fig. 15 (c), the primary current is cut off and the EHC is not able to extract energy from then on. v_{SC} and v_{DCDC_IN} fall with the discharging of storage capacitor gradually. In the stopping period as shown in Fig. 15 (a) between cursors a and b, the battery power replaces harvested energy to supply load at the time when the cursor points to a. Then, v_{DCDC_IN} maintains in V_{BAT} while v_{SC} gradually falls. At the time, when cursor points to b, the EHC receives the stopping order from superior controller making battery stop discharging. The experiment indicates that segmented voltage control principle solves the ''false startup'' problem and shortens start-up time significantly. Also, it distributes harvesting energy to capacitor storage energy, battery energy, and load consuming energy and provides stopping control interface for superior controller.

V. APPLICATION AND OPERATIONAL TESTS

The designed EHC in this paper is applied to the power management system of an online monitoring sensor unit. The sensor is used for monitoring the status of the ultra-high voltage shunt compensation capacitor bank (UHV-SCCB) at the 110kV side of main transformer in UHV-AC substation. In order to verify the running condition of EHC, a whole startup-running-stop process of the monitoring sensor is tested powered by the EHC.

A. AN APPLICATION OF EHC

The sensor is installed on the tower of UHV-SCCB, where the primary loop of the EHC is the electrode connecting line of capacitor. Aiming at the specific application scenario, a special shell mechanism containing the EHC and sensors is designed to solve the installation problem. As shown in Fig. 16, the shell mechanism uses aluminum materials and comprises the main part, one feedthrough aluminum bar and two buckles. The two ends of the feedthrough aluminum bar are fastened to the electrodes of capacitors making it replace the connecting line. The harvesting CT is encapsulated by epoxy (EP) inside the cylindrical groove in the main part.

The design structure of the monitoring sensor unit powered by the EHC is shown in Fig. 17. The monitoring sensor unit is designed to monitor the running status of UHV-SCCB and it has the functions of fundamental current monitoring, harmonic current content detection, waveform of transient current recording and storage, and wireless communication. As shown in Fig. 16, the monitoring sensor unit is composed

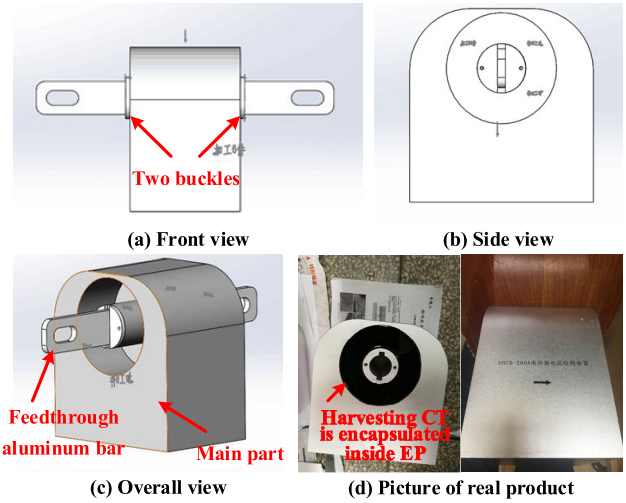

FIGURE 16. The shell mechanism of the monitoring sensor unit powered by EHC.

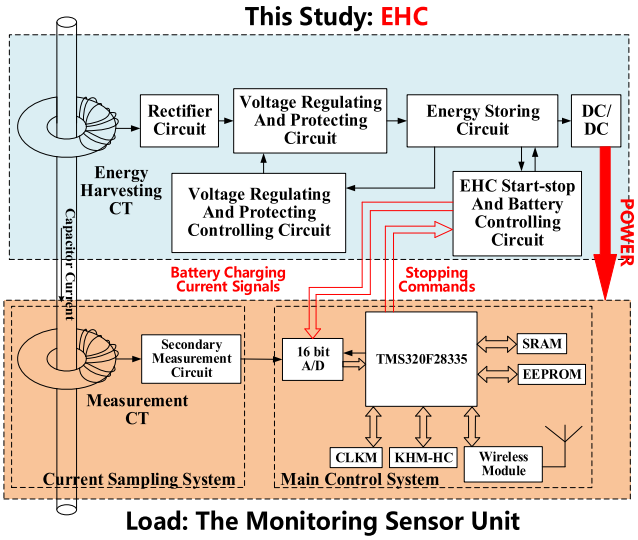

FIGURE 17. The design structure of the monitoring sensor unit powered by EHC.

of current sampling system and main control system. The former samples the capacitor current signals and converts them into voltage signals. The latter realizes data signal processing, data calculating, data saving, and wireless communication. Also, the main control system of the sensor samples the battery charging current signals of the EHC and gives the stopping commands to the EHC, which provides power support to the whole system.

The normal operation of the EHC is the foundation for the monitoring sensor unit to realize its functions. At any running stage of the sensor, the EHC will make it work normally and powered well. When UHV-SCCB switches or short-circuit fault occurs, the energy harvesting CT of the EHC short-circuits its secondary side immediately to bypass surge current to protect the monitoring sensor unit against any possible danger. And the EHC adjusts the balance between the

harvested power and the load consumed power in real time. Also, the EHC makes the monitoring sensor unit accomplish rapid auto-startup to record the switching waveform. After the EHC starts up, it can keep running to record different abnormal transient current, even if the capacitor current is too small to allow the EHC to extract enough energy. Besides, if UHV-SCCB is switched out, the main control system of the monitoring sensor unit can give stopping orders after sampling the primary current signals and battery charging current signals so as to avoid battery depletion. In general, battery maintains in floating charge.

B. THE OPERATIONAL TESTS OF EHC

To verify the running condition of the EHC, the function of recording the waveform of transient current is tested by monitoring the communication between the sensor and its upper computer. And the transmitted data is prolix because data of each waveform consists of hundreds of data frames. After extracting the recorded data in the communication frame by removing useless information like packet header, address, data type, data length, check code, and packet tail, the recorded waveforms could be drawn. Fig. 18 (a), Fig. 18 (b), and Fig. 18 (c) show the recorded waveforms of capacitor current by monitoring sensor unit in the start-up period, the running period, and the stopping period, respectively. In Fig. 18 (a), when the capacitor bank switches in, the capacitor current turns into oscillation from zero suddenly. The transient oscillation process continues for two cycles and the peak value of surge current is about 450A. Then, the capacitor current turns into AC steady state at 50Hz with the amplitude of about 100A. During the startup period, the EHC starts up rapidly to ensure the monitoring sensor unit's recording of transient waveforms, and prevents the sensor from being damaged from the surge current. In Fig. 18 (b), when the capacitor bank runs steadily, the capacitor current maintains in AC steady state at 50Hz with the amplitude of about 100A. The EHC harvested power continually supplies the sensor and the EHC adjusts the power balance in real time. In Fig. 18 (c), when the capacitor bank switches out, the capacitor current turns into zero. The EHC switches to the condition of battery power supplying, which enables the monitoring sensor unit to record the waveforms in the stopping period. To prevent battery from being depleted, the EHC is controlled to shut down after the capacitor bank stops for a while.

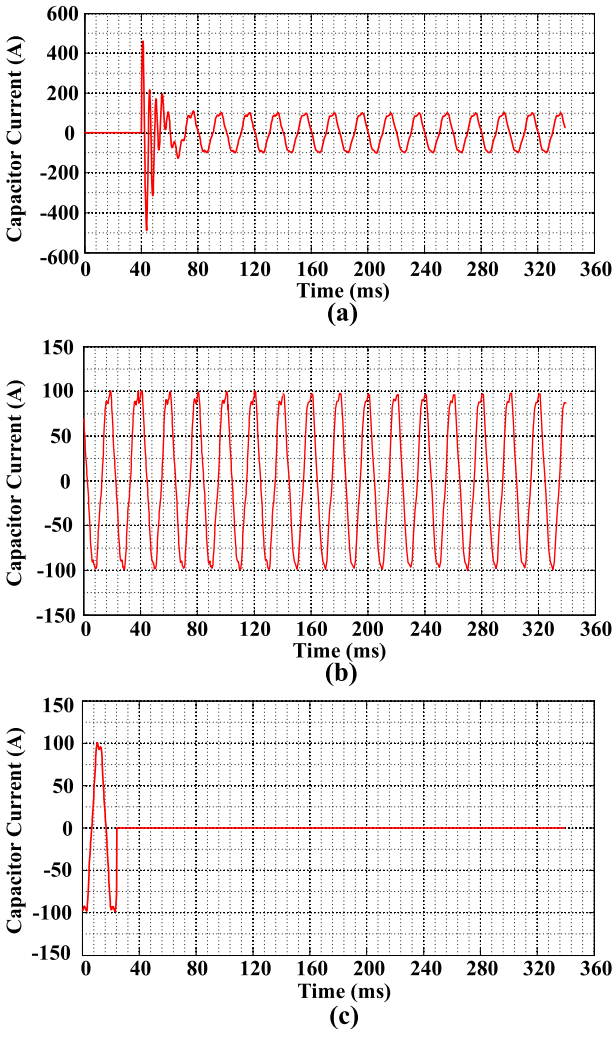

FIGURE 18. Recorded waveforms of capacitor current by monitoring sensor unit in different stages: (a) Recorded waveforms of capacitor current by monitoring sensor unit in the start-up period, (b) Recorded waveforms of capacitor current by monitoring sensor unit in the running period, (c) Recorded waveforms of capacitor current by monitoring sensor unit in the stopping period.

UHV-SCCB is assembled at the low voltage side of the main transformer in UHV substation. When harmonic wave occurs in power system due to power quality, transformer saturation, or some electric equipment that could cause waveform distortion, the capacitor voltage would distort. Due to the capacitivity of the capacitor, when the capacitor is in parallel with the inductive load, harmonic current would be generated and amplified. Therefore, it could be figured out that there are some distortions in the recorded current waveforms.

VI. CONCLUSION

This paper presents a high-reliability CT-based EHC supplying power to the monitoring sensors in power system. A comparison table is drawn to compare several conventional energy harvesting works with the EHC in this paper as shown in Table 6.

After comparing with the conventional works in Table 6, the novelties of the EHC could be summarized as follows:

(a) Differing from the circuits discussed in the previous studies, the EHC in this work accomplishes the integration of surge current protection, power balance adjustment, and autosensing controllable startup-running-stop management. And the EHC possesses the capacity of extracting the energy with a wide range from 12W under 80A_{rms} primary current to 50mW under 8.5A_{rms} primary current. Besides, the EHC employs only analog electronic components without digital ones, which makes it both simple and low-cost.

TABLE 6. Comparison among several conventional energy harvesting works with The EHC ('×' means not considered).

Contrastive CT EH Works	Surge Protection	Power Balance Adjustment	Startup-Stop Management		Order of Magnitudes of Harvested Power	Circuit Element Type
			Start-up Time	Controllable Stop		
[5]	×	×	×	×	10mW under 13.5A_{rms} primary current	All analog elements without digital ones
[16]	10Ω dissipative resistor	LDO controlled power balance with 4.95V~5V	1s	×	63.72mW under 10A_{rms} primary current	Analog and digital (LDO S-1313A33) elements
[17]	Zener Diode	×	×	×	300μW under magnetic flux density of 18μT_{rms}	Analog and digital (Amplifier LT1017) elements
[18]	×	×	×	×	From 1W to 5W	All analog elements without digital ones
[19]	×	×	×	×	612μW under magnetic flux density of 7μT_{rms}	Unknown
[20]	Nearly short-circuit with an NMOS	Voltage regulator controlled power balance	×	×	7.5mW from a 90W-60Hz desk lamp	Analog and digital (Amplifier) elements
EHC In This Work	Nearly short-circuit with 30mΩ dissipative resistor	Specific power balance adjusting circuit with 15~19V	Several milliseconds start-up time	Stopping control interface	From 12W under 80A_{rms} primary current to 50mW under 8.5A_{rms} primary current	All analog elements without digital ones

(b) Different from the traditional scheme of adopting transient protecting elements like Zener diode, TVS, or SPD, the EHC bypasses the strong current coupled to secondary side by primary surge current using a by-passing branch whose dissipative resistor is 30mΩ for current surge protection. When the surge current occurs in the primary loop, CT is short-cut at the secondary side, where the assembled analog elements are able to withstand the transient impact with decuple magnitudes.

(c) By regulating switching-on duration t_{on} and switching-off duration t_{off}, the EHC makes the harvested power synchronize with the consumed power. The energy harvesting capacity of the EHC is optimized by modulating returning voltage V_{RET} and operating voltage V_{OPT} to higher values, which expand the range of the harvested energy. Such procedure provides a practical method to adjust the power balance in energy harvesting applications.

(d) Different from conventional works, this study considers the segmented voltage control principle, which realizes autosensing controllable startup-running-stop management. Therefore, the EHC solves the problem of ''false startup'' and significantly shortens the start-up time to milliseconds and provides stopping control interface for superior controller.

REFERENCES

[1] R. Rosa, P. Livreri, C. Trigona, L. Di Donato, and G. Sorbello, ''Strategies and techniques for powering wireless sensor nodes through energy harvesting and wireless power transfer,'' *Sensors*, vol. 19, no. 12, p. 2660, Jun. 2019.

[2] T. Radil, P. M. Ramos, F. M. Janeiro, and A. C. Serra, ''PQ monitoring system for real-time detection and classification of disturbances in a single-phase power system,'' *IEEE Trans. Instrum. Meas.*, vol. 57, no. 8, pp. 1725–1733, Aug. 2008.

[3] Z. Li, H. Mei, and L. Wang, ''A power supply technology for a low-power online monitoring sensor based on electric field induction,'' *Sensors*, vol. 19, no. 9, pp. 2169–2170, May 2019.

[4] S. Lele, R. Sobot, and T. Sidhu, ''Piezoelectric transformer based disturbance monitoring methodology for high-voltage power supply lines,'' *IEEE Sensors J.*, vol. 14, no. 5, pp. 1425–1434, May 2014.

[5] R. H. Bhuiyan, R. A. Dougal, and M. Ali, ''A miniature energy harvesting device for wireless sensors in electric power system,'' *IEEE Sensors J.*, vol. 10, no. 7, pp. 1249–1258, Jul. 2010.

[6] Y.-K. Teh and P. K. T. Mok, ''Design of transformer-based boost converter for high internal resistance energy harvesting sources with 21 mV self-startup voltage and 74% Power Efficiency,'' *IEEE J. Solid-State Circuits*, vol. 49, no. 11, pp. 2694–2704, Nov. 2014.

[7] Y.-K. Teh and P. K. T. Mok, ''DTMOS-based pulse transformer boost converter with complementary charge pump for multisource energy harvesting,'' *IEEE Trans. Circuits Syst. II: Exp. Briefs*, vol. 63, no. 5, pp. 508–512, May 2015.

[8] H. Gonçalves, M. Martins, and J. Fernandes, ''Fully integrated energy harvesting circuit with -25-dBm sensitivity using transformer matching,'' *IEEE Trans. Circuits Syst. II: Exp. Briefs*, vol. 62, no. 5, pp. 446–450, May 2015.

[9] J. Zhang, P. Li, Y. Wen, F. Zhang, and C. Yang, ''A management circuit with upconversion oscillation technology for electric-field energy harvesting,'' *IEEE Trans. Power Electron.*, vol. 31, no. 8, pp. 5515–5523,' Aug. 2016.

[10] M. J. Moser, T. Bretterklieber, H. Zangl, and G. Brasseur, ''Strong and weak electric field interfering: Capacitive icing detection and capacitive energy harvesting on a 220-kV high-voltage overhead power line,'' *IEEE Trans. Ind. Electron.*, vol. 58, no. 7, pp. 2597–2604, Jul. 2011.

[11] J. C. Rodríguez, D. G. Holmes, and B. Mcgrath, ''A self-triggered pulsed-mode flyback converter for electric-field energy harvesting,'' *IEEE J. Emerg. Sel. Topics Power Electron.*, vol. 6, no. 1, pp. 377–386, Mar. 2018.

[12] O. Cetinkaya and O. B. Akan, ''Electric-field energy harvesting from lighting elements for battery-less Internet of Things,'' *IEEE Access*, vol. 5, pp. 7423–7434, 2017.

[13] A. Dolgov, R. Zane, and Z. Popović, ''Power management system for online low power RF energy harvesting optimization,'' *IEEE Trans. Circuits Syst. I, Reg. Papers*, vol. 57, no. 7, pp. 1802–1811, Jul. 2010.

[14] E. Ferro, V. M. Brea, P. López, and D. Cabello, ''Micro-energy harvesting system including a PMU and a solar cell on the same substrate with cold startup from 2.38 nW and input power range up to 10 μW using continuous MPPT,'' *IEEE Trans. Power Electron.*, vol. 34, no. 6, pp. 5105–5116, Jun. 2019.

[15] H. Shao, X. Li, C.-Y. Tsui, and W.-H. Ki, ''A novel single-inductor dual-input dual-output DC–DC converter with PWM control for solar energy harvesting system,'' *IEEE Trans. Very Large Scale Integr. (VLSI) Syst.*, vol. 22, no. 8, pp. 1693–1704, Aug. 2014.

[16] Z. Wu, Y. Wen, and P. Li, "A power supply of self-powered online monitoring systems for power cords," *IEEE Trans. Energy Convers.*, vol. 28, no. 4, pp. 921–928, Dec. 2013.

[17] N. M. Roscoe and M. D. Judd, "Harvesting energy from magnetic fields to power condition monitoring sensors," *IEEE Sensors J.*, vol. 13, no. 6, pp. 2263–2270, Jun. 2013.

[18] Z. Dai, J. Wang, Y. Li, Y. He, Z. Fang, and H. Hou, "Optimal design of magnetic coupling wireless power supply system for monitoring equipment," *IEEE Access*, vol. 6, pp. 58600–58608, 2018.

[19] S. Yuan, Y. Huang, J. F. Zhou, Q. Xu, C. Y. Song, and G. Yuan, "A high-efficiency helical core for magnetic field energy harvesting," *IEEE Trans. Power Electron.*, vol. 32, no. 7, pp. 5365–5376, Jul. 2017.

[20] J. Moon, J. Donnal, J. Paris, and S. B. Leeb, "A magnetically self-powered sensor node capable of wireless transmission," in *Proc. 28th Annu. IEEE Appl. Power Electron. Conf. Expo. (APEC)*, Mar. 2013, pp. 3151–3159.

[21] L. Du, C. S. Wang, X. Li, L. Yang, Y. Mi, and C. Sun, "A novel power supply of online monitoring systems for power transmission lines," *IEEE Trans. Ind. Electron.*, vol. 57, no. 8, pp. 2889–2895, Dec. 2010.

[22] F. Yang, L. Du, D. Wang, C. Wang, and Y. Wang, "A novel self-powered lightning current measurement system," *IEEE Trans. Ind. Electron.*, vol. 65, no. 3, pp. 2745–2754, Mar. 2018.

[23] G. Wang, C. Luo, H. Hofmann, and L. Rome, "Power electronic circuitry for energy harvesting backpack," in *Proc. IEEE Energy Convers. Congr. Expo. (ECCE)*, Sep. 2009, pp. 3544–3549.

[24] R. S. de Andrade Ferreira, J. F. de Araujo, F. L. M. Andrade, E. G. Costa, and F. C. F. Guerra, "Influence of electromagnetic forces in the gaps of a protective CT," *IET Sci. Meas. Technol.*, vol. 12, no. 7, pp. 872–877, Oct. 2018.

[25] R. Hunt, "Impact of CT errors on protective relays—Case studies and analysis," *IEEE Trans. Ind. Appl.*, vol. 48, no. 1, pp. 52–61, Jan./Feb. 2012.

[26] *Instrument Transformers—Part 2: Additional Requirements for Current Transformers*, document IEC 61869-2:2012, 2012.

[27] *IEEE Standard Requirements for Instrument Transformers*, Standard C57.13-2016, 2016.

[28] N. Michelusi, K. Stamatiou, and M. Zorzi, "Transmission policies for energy harvesting sensors with time-correlated energy supply," *IEEE Trans. Commun.*, vol. 61, no. 7, pp. 2988–3001, Jul. 2013.

[29] H. Liu, Z. Ji, T. Chen, L. Sun, S. C. Menon, and C. Lee, "An intermittent self-powered energy harvesting system from low-frequency hand shaking," *IEEE Sensors J.*, vol. 15, no. 9, pp. 4782–4790, Sep. 2015.

[30] S. Chamanian, S. Baghaee, H. Uluşan, Ö. Zorlu, E. Uysal-Biyikoglu, H. Külah, "Implementation of energy-neutral operation on vibration energy harvesting WSN," *IEEE Sensors J.*, vol. 19, no. 8, pp. 3092–3099, Apr. 15, 2019.

[31] M. M. Mnif, H. Mnif, and L. Mourad, "A dual frequency RF-DC rectifier circuit with a low input power for radio frequency energy harvesting," *J. Circuits Syst. Comput.*, vol. 28, no. 3, Mar. 2019, Art. no. 1950048.

[32] N. A. K. Z. Abidin, N. M. Nayan, M. M. Azizan, and A. Ali, "Analysis of voltage multiplier circuit simulation for rain energy harvesting using circular piezoelectric," *Mech. Syst. Signal Process.*, vol. 101, pp. 211–218, Feb. 2018.

[33] T. Lim and Y. Kim, "Compact self-powered wireless sensors for real-time monitoring of power lines," *J. Electr. Eng. Technol.*, vol. 14, no. 3, pp. 1324–1326, May 2019.

[34] K. Kutluay, Y. Cadirci, Y. S. Ozkazanc, and I. Cadirci, "A new online state-of-charge estimation and monitoring system for sealed lead-acid batteries in Telecommunication power supplies," *IEEE Trans. Ind. Electron.*, vol. 52, no. 5, pp. 1315–1327, Oct. 2005.

[35] K.-S. Yoon, S.-W. Hong, and G.-H. Cho, "Double pile-up resonance energy harvesting circuit for piezoelectric and thermoelectric materials," *IEEE J. Solid-State Circuits*, vol. 53, no. 4, pp. 1049–1060, Apr. 2018.

JUE HOU received the B.E. degree from the School of Electrical and Electronic Engineering, Huazhong University of Science and Technology, Wuhan, China, in 2016, where he is currently pursuing the Ph.D. degree.

His research interests include monitoring and evaluation of distribution networks, smart grid, and power system operation and control.

SHAORONG WANG received the B.S. degree from Zhejiang University, Hangzhou, China, in 1984, the M.S. degree from North China Electric Power University, Baoding, China, in 1990, and the Ph.D. degree from the Huazhong University of Science and Technology, Wuhan, China, in 2004, where he is currently a Professor with the School of Electrical and Electronic Engineering.

His current research interests include power system operation and control, smart grid, robotic application, big data, and machine vision.

SHUWEI ZHANG received the B.E. degree from the School of Electrical and Electronic Engineering, Huazhong University of Science and Technology, Wuhan, China, in 2015, where she is currently pursuing the master's degree. Her research interests include artificial intelligence, mechanical structure and operation of secondary system of intelligent substation.

QIAN SHE received the B.E. degree from the School of Electronic Engineering, Huazhong University of Science and Technology, Wuhan, China, in 2017, where she is currently pursuing the master's degree.

Her research interests include power system operation and control, smart grid, and artificial intelligence.

YUXIN ZHU received the B.E. degree from the School of Electrical and Electronic Engineering, Huazhong University of Science and Technology, Wuhan, China, in 2017, where she is currently pursuing the master's degree.

Her research interests include electric vehicle planning and smart grid, and optimal control of smart distribution systems.

CHENGJING LI received the B.E. degree from the School of Electrical and Electronic Engineering, Huazhong University of Science and Technology, Wuhan, China, in 2017, where he is currently pursuing the master's degree. His research interests include software design on evaluation and optimization of active distribution networks.